Journal of Electromyography and Kinesiology 84 (2025) 103046

Contents lists available at ScienceDirect

Journal of Electromyography and Kinesiology

journal homepage: www.elsevier.com/locate/jelekin

Passive stretching-induced changes in the spatial distribution of muscle excitation: A step forward in the interpretation of the underlying mechanisms

Nicholas Toninelli, Giuseppe Coratella, Christian Doria, Eloisa Limonta, Marta Borrelli, Susanna Rampichini, Fabio Esposito, Stefano Longo [1,*], Emiliano Cè [1]

Department of Biomedical Sciences for Health (SCIBIS), Università degli Studi di Milano, via G. Colombo 71, 20133 Milan, Italy

ARTICLE INFO

Keywords:
High density surface electromyography
Elongation
Plantar-flexor muscles
Muscle architecture
Discomfort perception

ABSTRACT

We assessed passive static stretching (PS) effects on the spatial distribution of muscle excitation (SDME) of the stretched (SL) and contralateral non-stretched limb (CL) during maximum voluntary isometric contractions (MVC). Before (PRE) and after 5-min PS, immediately (POST), at min 5 ($POST_5$) and 10 ($POST_{10}$), range of motion (ROM), maximal M−wave (M_{max}) and MVC of both limbs were assessed in thirty men. During MVC, high-density surface electromyographic signals from the *gastrocnemius medialis* (GM) and *lateralis* (GL) were collected. The root mean square (RMS) and centroid coordinates were then obtained. During PS, discomfort perception (VAS), proximal and distal GM architecture were recorded. At POST, ROM increased and MVC decreased together with RMS in both limbs ($P < 0.05$). A cranio-caudal shift in SDME occurred in both muscles of SL and CL ($P < 0.01$) that persisted only in SL until $POST_5$ in GM ($P = 0.04$), and $POST_{10}$ in GL ($P = 0.01$). During PS, VAS was high (>8.0), and fascicle length and angle increased from rest ($P < 0.01$). No differences between GM portions were found in muscle architecture and in M_{max} ($P > 0.05$). The results suggest involvement of central neural mechanisms in SDME shift. The prolonged effect in SL compared to CL indicates a possible additional contribution from mechanical mechanisms.

1. Introduction

Passive stretching (PS) is widely performed in sport and rehabilitation mainly to improve joint range of motion (ROM) (Bryant et al., 2023). Nonetheless, acute PS can negatively impact the stretched muscle function, reducing its force-generating capacity (Behm et al., 2021c). This is often accompanied by a decrease in surface electromyographic signal (sEMG) amplitude from the stretched muscle (Trajano et al., 2017) arising from changes in perceptual, neural, and mechanical components (Behm et al., 2021a; Trajano and Blazevich, 2021).

The most common technique employed to non-invasively assess muscle electric activity is bipolar sEMG (Campanini et al., 2022; Merletti and Farina, 2016). One of the drawbacks of this technique is that sEMG signal is detected on a limited muscle area, thus restricting the spatial information that can be obtained on the muscle of interest, including regional activation and single motor unit activity (Campanini et al., 2022; Merletti and Farina, 2016). Recently, the development of high-density sEMG (HD-sEMG) has made possible to detect the electrical signal from a large portion of the muscle, allowing the analysis of a wide muscle area. This technique provides a 2-D map generation of all electrodes, where the weighted average of the raw or rectified signal is quantified using a pair of coordinates forming a centroid, thus reflecting the spatial distribution of muscle excitation (SDME) (Dideriksen et al., 2016; Falla et al., 2017; Falla and Gallina, 2020). Interestingly, the use of HD-sEMG allowed a more detailed analysis of the previously reported PS-induced alterations in muscle excitation (Hirono et al., 2025; Maeda et al., 2021; Mazzo et al., 2021). Indeed, PS-induced modifications of motor units' behavior of the stretched muscle were observed during submaximal isometric contractions. Specifically, Mazzo et al. (Mazzo et al., 2021) reported an increase in neural drive following a five-minute PS intervention. Maeda and colleagues (Maeda et al., 2021) observed variations in *gastrocnemius medialis* muscle (GM) SDME subsequent to PS across different levels of contraction, providing evidence for a spatial reorganization of motor unit activity. Additionally, Hirono and

* Corresponding author at: Department of Biomedical Sciences for Health (SCIBIS), University of Milan, Via Colombo 71, 20133 Milan, Italy.
E-mail address: stefano.longo@unimi.it (S. Longo).
[1] These authors contributed equally to this work and share last authorship.

https://doi.org/10.1016/j.jelekin.2025.103046
Received 13 March 2025; Received in revised form 22 July 2025; Accepted 1 August 2025
Available online 5 August 2025

colleagues highlighted modulations of neural drive in non-stretched vastus lateralis muscle following selective stretching of synergist rectus femoris (Hirono et al., 2025). However, the mechanisms underlying such behavior are still unclear. The authors hypothesized peripheral and central neural adaptations, as well as mechanical changes of the stretched-tissue properties, thus influencing the motor unit recruitment strategies and emphasizing an inhomogeneous muscle activation pattern during submaximal contractions (Maeda et al., 2021). Whether these PS-induced changes in SDME occur during maximal contractions and which mechanisms (e.g., neural and/or mechanical) contribute to this phenomenon have not been yet investigated. By assessing cross-over effects in SDME through HD-sEMG recordings in the contralateral non-stretched limb, it is possible to evaluate the relative contributions of neural and mechanical factors to the acute neuromuscular response to PS (Cè et al., 2020). Therefore, the present study aimed to assess the effects of PS on SDME during maximal isometric contractions in both the stretched and homologous contralateral non-stretched muscle groups. Investigating these changes will enhance our understanding of how passive joint mobilization influences force production, ultimately optimizing stretching routines for both exercise and rehabilitation contexts.

2. Methods

2.1. Participants

To compute the required *a priori* sample size, we deemed the PS-induced strength loss in the contralateral non-stretched limb (CL) as main outcome (Coratella et al., 2021). A commercially available statistical software (G-Power 3.1, Dusseldorf, Germany) was used with the following parameters: $\alpha = 0.05$, required power $(1\text{-}\beta) = 0.80$, repeated measures analysis of variance (ANOVA-RM) design, Cohen's *d* effect size (ES) = 0.96 (Coratella et al., 2021). The sample size resulted in 22 participants. To ensure sufficient statistical power, we enrolled 30 healthy male volunteers [age: 24 ± 2 years, stature: 1.78 ± 0.07 m, body mass: 77 ± 6 kg (mean ± SD)]. Participants were asked to refrain from intense physical activity at least in the 48 h prior evaluations and to avoid ergogenic foods and beverages in the previous 24 h. All the participants gave their written informed consent. The study was performed in accordance with the latest principles of the Declaration of Helsinki and approved by the local University Ethics Committee (CE 84/23).

2.2. Study design

All sessions took place in a room at constant temperature (22 ± 1°C) and humidity (50 ± 3 %). Tests were performed at the same time of the day between 9.00 and 12.00 a.m., to limit the effect of circadian rhythms on muscle strength and joint mobility (Gifford, 1987).

A schematic representation of the study design is given in Fig. 1. This investigation was conceived as a within-subject cross-sectional study, consisting in three experimental sessions separated by at least 72 h. Briefly, the first session (day1) served as familiarization, in which participants got accustomed with the experimental set up and procedures. Reference points along with some skin landmarks were drawn on transparent sheets for ensuring consistency in angle transducer, HD-sEMG matrix, and stimulation electrodes repositioning. The dominant limb (right for all participants) was designated as the stretched limb (SL), while the non-dominant limb served as the CL for cross-over evaluation. This limb assignment was maintained consistently throughout the protocol. The remaining two sessions (day2 and day3) were randomized.

In each session, and for the entire duration of the experiment, participants were asked to lie prone on a custom-made dynamometer, with the hip in the neutral position and knee joints fully extended. The ankle was positioned in a movable metal plate and secured with Velcro® straps (Velcro Industries Inc., Willemstad, Netherlands Antilles) to minimize heel movement (Longo et al., 2021). The metal plate was connected to a load cell (model SM-2000 N, Interface, UK; operating linearly between 0 and 2000 N), aligned with the force axis and previously calibrated. Both day2 and day3 began with the control condition, during which measurements were taken before (PRE), immediately after (POST), and at 5 ($POST_5$) and 10 min ($POST_{10}$) following a 5 min rest period. Ten min after the last control measurement, the intervention condition was initiated. In this phase, the same measurements were collected at the same time points; however, a 5-min PS protocol was administered in place of the rest period.

At each time point, the following assessments were conducted in the same order: ankle dorsiflexion ROM, maximal M−wave (M_{max}), maximum voluntary isometric contraction (MVC) of the plantar flexor muscles, together with HD-sEMG signals from the GM and *gastrocnemius lateralis* (GL). On one day, the direct effects of PS were assessed by performing all measurements on the SL, while on the other day, cross-over effects were evaluated by performing the measurements on the CL, along with an assessment of GM muscle architecture during the PS

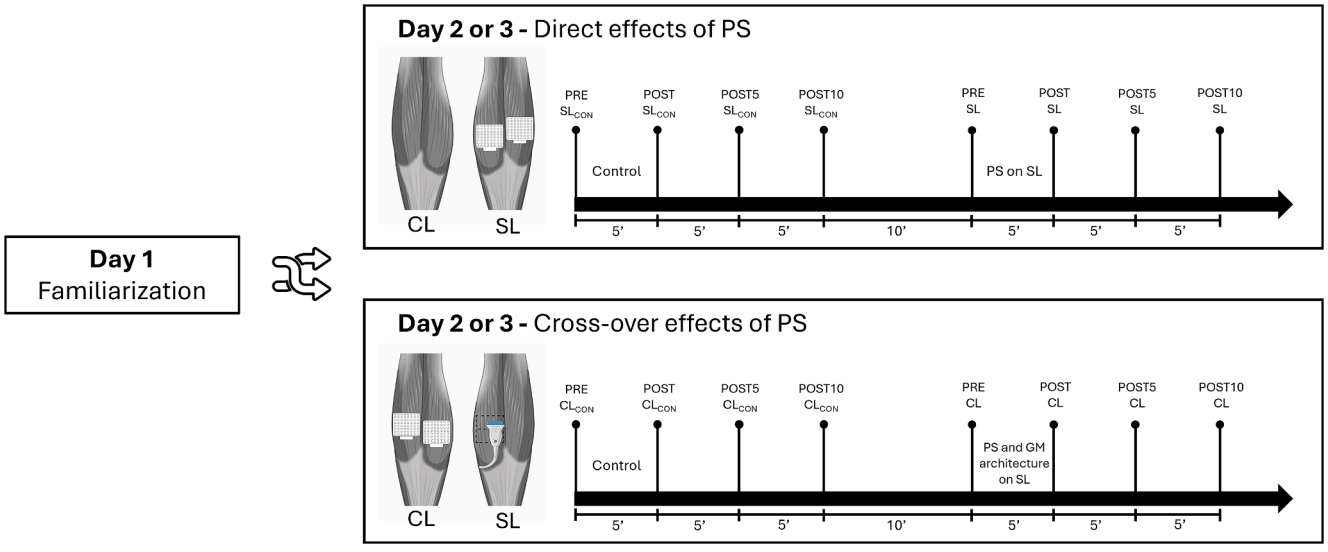

Fig. 1. Schematic representation of the study design. PS: passive stretching; GM: *gastrocnemius medialis*; SL: stretched limb; CL: contralateral non-stretched limb; CON: control.

protocol (see details below).

2.3. Measurements and data analysis

Fig. 2 illustrates the experimental set-up used during the measurements and during the PS procedure.

2.3.1. Ankle dorsiflexion ROM

The ankle dorsiflexion ROM was assessed with participants in the prone position, with the hip in the neutral position and knee joints fully extended. A previously calibrated bi-axial angular transducer (mod. TSD130B, Biopac System Inc., Santa Barbara, CA, USA), positioned on the external face of the fibula and on the calcaneus was used to monitor the changes in ankle ROM. The ankle was dorsiflexed from the neutral position (i.e., tibia perpendicular to the calcaneus = 0° of dorsiflexion) up to the maximum point of discomfort reported by the participant. With the help of a metronome, the maneuver was completed in 6 s to avoid reflex contractions, constantly checking the HD-sEMG signal. The procedure was repeated three times at PRE and once at the other time points. The maximum joint ROM at each time point was selected for analysis.

2.3.2. Electrical nerve stimulation

M_{max} was recorded while maintaining the same prone position, with the ankle secured in the neutral position (0° dorsiflexion). The procedure was performed using a high-voltage electrical stimulator (Digitimer Stimulator Model DS7AH, Hertfordshire, UK). To obtain the M_{max}, a series of single rectangular pulses (100–150 V pulse of 1 ms in width) were delivered to the tibial nerve. The optimal stimulation site was first identified using a hand-held cathode electrode pen. The cathode (8-mm diameter, Ag-AgCl circle electrode; Medicompex SA, Ecublens, Switzerland) was placed on the popliteal fossa, while the anode (50 x 100 mm rectangular electrode; Medicompex SA, Ecublens, Switzerland) was positioned over the patella. Stimulations started from 30 mA and were progressively increased by 5 mA increments until M−wave no longer increased. To ensure supramaximal stimulation, the highest stimulation intensity was further increased by 20 % [stimulation current = 115 ± 15 mA]. M−waves were amplified and acquired in monopolar configuration, with a sampling rate of 2048 Hz (multichannel amplifier mod. EMG-USB, OtBioelettronica, Turin, Italy; input impedance: >90 MΩ; CMRR: >96 dB). M_{max} was calculated in the GM and GL by averaging the peak-to-peak M−waves of each individual channel corresponding to the upper (rows 1–4) and lower (rows 5–8) half of the 64-electrodes grids used for HD-sEMG detection.

2.3.3. Maximum voluntary isometric contractions

MVCs were assessed in the same position and with the same ankle configuration used for M_{max} measurements. After a standardized warm-up (10 2-s isometric submaximal contractions of increasing intensity up to around 70 % MVC) three MVCs were performed at PRE, and one at POST, $POST_5$ and $POST_{10}$. Participants were instructed to push as hard as possible and to maintain the contraction for about 4 s. Each attempt was separated by 2 min recovery to avert a possible effect of fatigue. Visual feedback was provided to the participants. The force signal was digitized, (mod. UM 150, Biopac, Biopac System Inc., Santa Barbara, CA, USA), sampled at 2048 Hz, and directed to an auxiliary input of the electromyography amplifier (mod. EMG-USB, OtBioelettronica, Turin, Italy). Data were subsequently analyzed offline using Otbiolab+ software, considering the average value over the middle second of the force plateau. Torque was obtained by multiplying the force value times the distance between the apical aspect of the external malleolus and the force application point. At PRE, the highest torque recorded was used for data analysis.

2.3.4. HD-sEMG and centroid coordinates

The HD-sEMG signal was detected in both SL and CL during MVC assessments. The skin was shaved, gently scrubbed with abrasive gel (Nuprep, Weaver and Co., Aurora, USA), and cleaned with alcohol to minimize the skin-electrode impedance (<2000 Ω). Afterwards, two semi-disposable 8 × 8 electrode grids of 64 electrodes (GR10MM0808 model, 94 × 94 mm, inter-electrode distance of 10 mm, OtBioelettronica, Turin, Italy) were placed upon the GM and GL (Barbero et al., 2012). The grid-skin interface consisted of double-sided, cylindrical punctured adhesive foam, filled with semisolid conductive paste (AC cream, Spes Medica, Battipaglia, SA, Italy). HD-sEMG signals were acquired in monopolar configuration, amplified with a sampling rate of 2048 Hz (multichannel amplifier mod. EMG-USB, OtBioelettronica, Turin, Italy; input impedance: >90 MΩ; CMRR: >96 dB) and collected on a personal computer. The raw signals were digitally filtered with a IV-order Butterworth filter with a band pass of 10–500 Hz and processed in time domain within the 1-s period of the corresponding MVC plateau. After visual inspection, signals of channels containing artifacts were

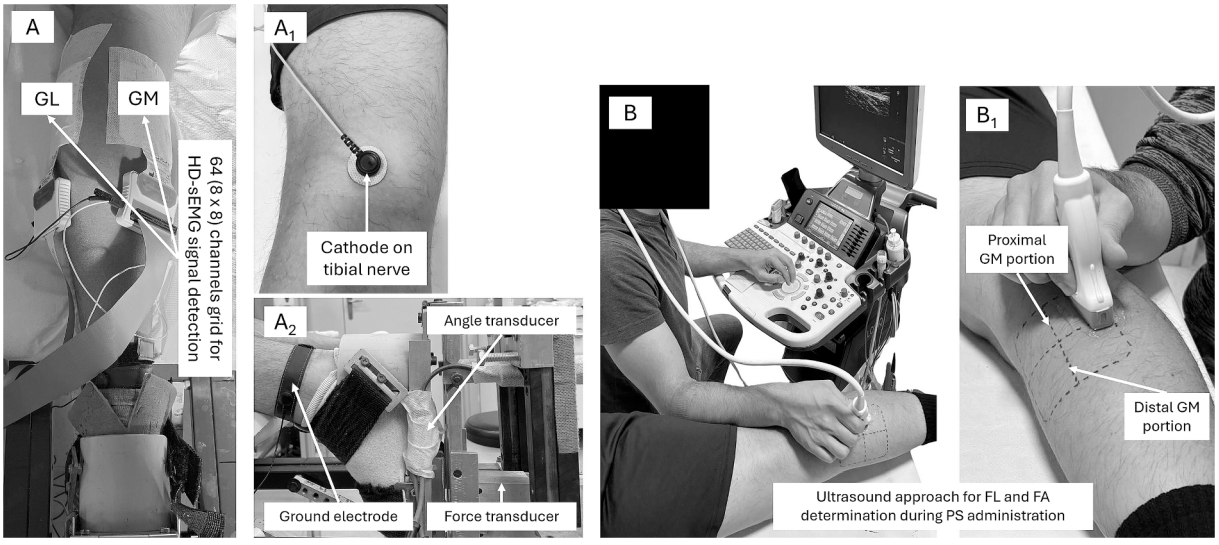

Fig. 2. Experimental setup representation of high-density surface electromyography (HD-sEMG) matrix placement over *gastrocnemius medialis* (GM) and *gastrocnemius lateralis* (GL) (panel A) for electrophysiological parameters recording and cathod placement on the popliteal fossa for electrical stimulation procedure (panel A1); detail of the movable metal plate connected to the load cell (panel A2). Ultrasound assessment during passive stretching procedure (panel B) for proximal and distal muscle architecture evaluations (panel B1). FL: fascicle length; FA: fascicle angle; PS: passive stretching.

exported as .CSV for processing in Excel software (Microsoft Corporation, Redmond, WA, USA). Low quality channels were removed and replaced by averaging the values of the two adjacent channels in the same row, accounting for their position in the HD-sEMG matrix. The corrected signals were then reimported into Otbiolab+ for further analysis. The root mean square of the signal (RMS) was calculated in consecutive 250-ms time-windows and then averaged. HD-sEMG monopolar signals from channels located above the innervation zone were excluded from the analysis based on visual inspection.

The SDME was determined within the same time-window used for RMS definition. Changes in the centroid coordinates of the muscle excitation map provided by the Otbiolab+ software were then calculated. Briefly, the software estimates the voltage under each electrode and return the average squared values over the selected epoch by means of a centroid. Cranio-caudal (*x*-axis) and medio-lateral (*y*-axis) centroid coordinates were exported in 250-ms epochs, defined as modulus, and averaged. The magnitude of the displacement along the *x* and *y* axes was expressed as a percentage relative to the center of the HD-sEMG matrix, as shown in Fig. 3A.

2.3.5. Stretching and VAS

The stretching procedure consisted of five elongations administered by the same operator. The participant's plantar flexors were stretched to the point of discomfort, as verbally indicated by the participant, over a duration of 6 s guided by a metronome. Throughout the maneuvers, the ankle joint angle was continuously adjusted to ensure that the force exerted by the operator remained constant, as monitored by the load cell connected to the metal plate. During the final bout, participants reached an ankle dorsiflexion angle of 30 ± 2°. Each bout was held for 45 s and separated by 15 s of recovery, in which the ankle was moved to the initial position for a total duration of 5 min (Longo et al., 2021). Furthermore, we asked the participants to verbally indicate the perceived discomfort in both gastrocnemii before and during the last 15 s of each stretch. For this purpose, we used a 0 – 10 visual analogue scale (VAS) whose extremes represented "no discomfort" and "maximal discomfort" (Coratella et al., 2023).

2.3.6. GM muscle architecture

To assess whether differences in regional elongation of the stretched muscle may contribute to the muscle excitation centroid shift, GM architecture was assessed in a subsample of 23 participants [age: 24 ± 2 years, stature: 1.79 ± 0.06 m, body mass: 76 ± 7 kg (mean ± SD)]. Acquisitions were made on SL during PS as part of the CL intervention. The same GM area used for HD-sEMG detection was marked on the SL skin using a dermographic pen, corresponding to the matrix perimeter. This area was divided into an upper and lower region, corresponding to channel rows 1–4 and 5–8, respectively (Fig. 3B). PS was then administered to the SL. B-mode ultrasound images (LOGIQS7 GE©, Fairfield, Connecticut, USA) were collected in the upper and lower regions at rest and during the last 15 s of the first, third and fifth elongation using 5-cm linear-array probe (mod. 9L, 3.1–10.0 MHz). Due to the short acquisition time-window, the images were captured in GM only, assuming a similar behavior of the GL architecture (Aeles et al., 2022). To aid subsequent acquisitions, probe position was marked on the skin with a dermographic pen. Images were exported and analyzed offline using a public domain software (ImageJ 1.44b, National Institutes of Health, USA). Three muscle fascicles were identified per image. Fascicle length was measured from the deep to superficial aponeurosis, accounting for any curvature. If a fascicle portion was missing, its length was manually extrapolated (Franchi et al., 2018). Fascicle angle, defined as the insertion angle into the deep aponeurosis, was measured on the same fascicles. The average of the three fascicle lengths and angles was used for analysis.

2.4. Statistical analysis

Statistical analysis was performed using a statistical software package (IBM SPSS® Statistics 28, Armonk, NY, USA). Normality of the sample distribution was assessed applying the Shapiro-Wilk test. Sphericity was checked by the Mauchly's test. In case of violation, Greenhouse-Geisser correction was considered. Centroid coordinates PRE values of the intervention and control sessions were used to calculate the intraclass correlation coefficient (ICC) with 95 % of confidence interval (95 %CI) as a measure of relative inter-day reliability. The ICC was interpreted as excellent (≥0.90), good (0.89–0.70), moderate (0.69–0.50) or poor (≤0.49) (Koo and Li, 2016). Direct and cross-over PS-induced effects in ROM and MVC were assessed by a three-way ANOVA-RM (*time:* PRE, POST, $POST_5$, and $POST_{10}$; *condition*:

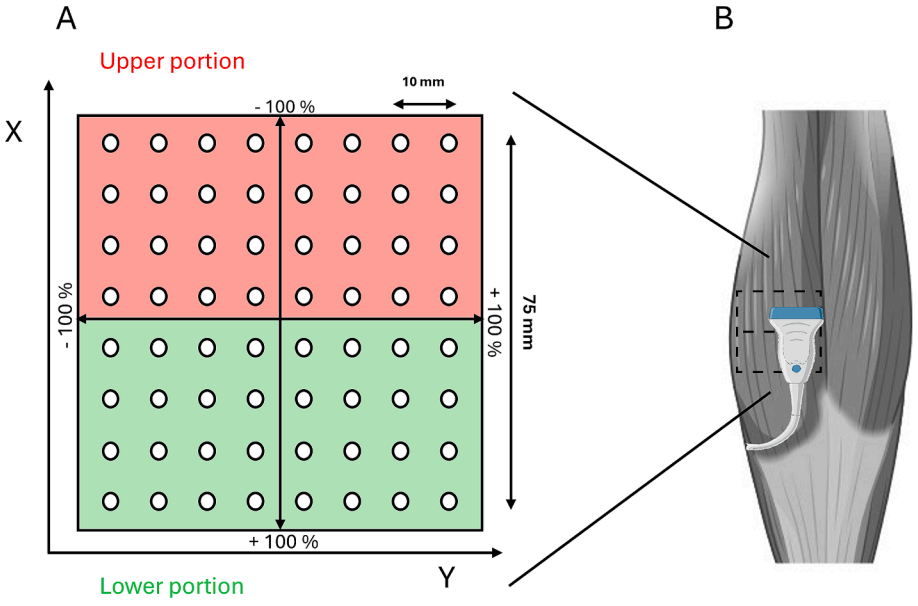

Fig. 3. Details of the high-density surface electromyographic grid dimensions, subdivision into upper and lower portions, and the axes considered for analyzing centroid displacement (panel A), along with the representation of the *gastrocnemius medialis* regions used to assess muscle architecture during PS (panel B). X: cranio-caudal axis; Y: medio-lateral axis.

intervention and control*; limb*: SL and CL). Direct and cross-over PS-induced effects in HD-sEMG RMS and centroid coordinates were assessed by a four-way ANOVA-RM (*time:* PRE, POST, $POST_5$, and $POST_{10}$; *condition*: intervention and control*; limb*: SL and CL; *muscle*: GM and GL). Direct and cross-over PS-induced effects in M_{max} were assessed by a five-way ANOVA-RM (*time:* PRE, POST, $POST_5$, and $POST_{10}$; *condition*: intervention and control*; limb*: SL and CL; *muscle*: GM and GL; *muscle portion:* upper and lower). Two-way ANOVA-RM was used to test the PS-induced differences in muscle architecture variables (*elongation:* PRE and elongation #1, #3, and #5; *GM muscle portion:* upper and lower). Friedman's two-way rank ANOVA with related samples was used to test differences in VAS (*elongation:* from #1 to #5; *muscle*: GM and GL). Multiple comparisons were adjusted using the Bonferroni's correction. The significance was set with $P < 0.05$. The magnitude of the interactions and main effects was calculated using partial eta squared (η_p^2), and was interpreted as small (0.01–0.059), medium (0.06–0.139), and large (≥0.14). The magnitude of the pairwise comparisons was determined using Cohen's *d* effect size (ES) with 95 %CI and interpreted as trivial (0–0.19), small (0.20–0.59), moderate (0.60–1.19), large (1.20–1.99) and very large (≥ 2.00) (Hopkins et al., 2009). Data are reported as mean ± SD if not otherwise specified.

3. Results

The ICC is reported in Table 1. The ICC ranged from *good* to *excellent* (0.83 to 0.99). To increase figures readability, the control session measurements were separately reported in Table 2.

3.1. Ankle dorsiflexion ROM

Changes in ankle ROM are presented in Fig. 4A. ANOVA-RM disclosed a *time* × *condition* × *limb* interaction in ROM ($F_{1.51} = 38.73$, $P = 0.010$, $\eta_p^2 = 0.17$, *large*). Compared to PRE, the ankle ROM increased in the SL from POST [5.87 ± 2.30°, $P < 0.001$, $ES = 2.50$ (1.76 to 3.23), *very large*] to $POST_{10}$ [1.75 ± 1.23° $P < 0.001$, $ES = 1.45$ (0.93 to 1.96), *large*]. In CL, ankle ROM increased only in POST by 2.43 ± 2.94° [$P < 0.001$, $ES = 0.83$ (0.41 to 1.24), *moderate*]. After stretching, ROM was greater in SL compared to CL at all time points [$P < 0.001$, *ES*-range = 0.83 (0.41 to 1.24), *moderate*]. No changes in ROM occurred in SL_{CON} and CL_{CON} ($P = 0.39$ and 0.62 in the two limbs, Table 2).

3.2. M_{max}

ANOVA-RM did not show a *time* × *condition* × *limb* × *muscle* × *muscle portion* interaction for M_{max} ($F_{1.12} = 0.96$, $P = 0.42$, $\eta_p^2 = 0.03$, *small*). No changes in M_{max} occurred in SL_{CON} and CL_{CON} in the two portions of both GM and GL (*P* from 0.51 to 1.00, Table 2).

3.3. MVC

Changes in MVC are shown in Fig. 4B. ANOVA-RM disclosed a *time* × *condition* × *limb* interaction in MVC ($F_3 = 10.67$, $P < 0.001$, $\eta_p^2 = 0.27$, *large*). Compared to PRE, the MVC decreased in SL from POST (16.62 ± 3.50 %, $P < 0.001$, $ES = -2.96$ (−3.79 to −2.11), *very large*] to $POST_{10}$ [4.67 ± 4.43 %, $P < 0.001$, $ES = -0.94$ (−1.34 to −0.54), *moderate*]. In CL, MVC decreased only in POST by 9.66 ± 8.14 % [$P < 0.001$, $ES = -1.26$ (−1.68 to −0.81), *large*]. After stretching, MVCs were lower in SL compared to CL at all time points [$P < 0.001$, *ES*-range = -0.75 (−1.15 to −0.34), *moderate*]. No changes in MVC occurred in SL_{CON} and CL_{CON} ($P = 0.57$ and 0.35 in the two limbs, Table 2).

3.4. HD-sEMG RMS during MVC

A *time* × *condition* × *limb* × *muscle* interaction was retrieved for HD-sEMG RMS ($F_{2.05} = 5.84$, $P = 0.005$, $\eta_p^2 = 0.17$, *large*). Compared to PRE, the GM HD-sEMG RMS (Fig. 5) decreased in SL by 8.88 ± 13.04 % in POST [$P = 0.003$, $ES = -0.60$ (−0.98 to 0.20), *moderate*]; the GL HD-sEMG RMS decreased from POST [10.03 ± 11.45 %, $P < 0.001$, $ES = -0.86$ (−1.29 to −0.44), *moderate*] to $POST_{10}$ [4.81 ± 7.22 %, $P < 0.001$, $ES = -0.57$ (−0.96 to −0.18), *small*]. In CL, the HD-sEMG RMS decreased only in POST by 9.13 ± 12.96 % [$P < 0.001$, $ES = -0.67$ (−1.06 to −0.27), *moderate*] and 9.89 ± 12.07 % [$P < 0.001$, $ES = -0.81$ (−1.22 to −0.39), *moderate*] in GM and GL, respectively. No changes in HD-sEMG RMS were detected in SL_{CON} and CL_{CON} ($P = 0.13$ and 0.10 in the two limbs, Table 2). To ensure that a possible shift in the centroid was not due to a local reduction in RMS of individual channels, we calculated the percentage difference in RMS between POST and PRE for each individual channel, as shown in Supplementary Fig. 1, and for each row, as highlighted in Supplementary Table 1.

3.5. Centroid coordinates

Changes for the *x*-axis (cranio-caudal direction) spatial coordinates of the HD-sEMG signal and representative activation maps showing HD-sEMG amplitudes are presented in Figs. 6 and 7, respectively. No *time* × *condition* × *limb* × *muscle* interaction was observed for the *x*-axis ($F_{2.07} = 1.20$, $P = 0.32$, $\eta_p^2 = 0.04$, *small*). *Time* × *condition* ($F_3 = 7.51$, $P = 0.003$, $\eta_p^2 = 0.15$, *large*) and *limb* × *muscle* ($F_1 = 5.22$, $P = 0.03$, $\eta_p^2 = 0.15$, *large*) interactions were retrieved. All the other interactions were not statistically significant (*P*-range: 0.12 – 0.78). Pairwise comparisons highlighted that in SL the centroid shifted caudally in both GM [$P = 0.003$, $ES = 0.59$ (0.20 to 0.97), *small*] and GL [$P < 0.001$, $ES = 0.78$ (0.36 to 1.18), *moderate*] in POST; the caudal shift persisted in GM until $POST_5$ [$P = 0.04$, $ES = 0.41$ (0.03 to 0.77), *small*] and in GL until $POST_{10}$ [$P = 0.01$, ES = 0.51 (0.13 to 0.87), *small*]. In CL, the centroid shifted caudally only in POST in both GM [$P = 0.001$, $ES = 0.67$ (0.26 to 1.06), *moderate*] and GL [$P = 0.002$, and 0.63 (0.23 to 1.01), *moderate*]. Changes for the *y*-axis (medio-lateral) spatial coordinates of the HD-sEMG signal are presented in Supplementary data set 1. No significant *time* × *condition* × *limb* × *muscle* interaction was found for the *y*-axis ($F_{1.80} = 2.49$, $P = 0.36$, $\eta_p^2 = 0.03$, *small*). No shift occurred in the centroid coordinates in SL_{CON} and CL_{CON} (*x*-axis, *P*-range: 0.29 – 0.71; *y*-axis, *P*-range: 0.24 – 0.88).

Table 1
Intersession reliability of centroid spatial coordinates presented as a percentage relative to the center (0) of the HD-sEMG matrix along the *x* (cranio-caudal) and *y* (medio-lateral) axis in the stretched and contralateral non-stretched limb.

	Stretched limb							Contralateral non-stretched limb						
	Trial 1		Trial 2					Trial 1		Trial 2				
Variable	mean	SD	mean	SD	ICC	95 %CI		mean	SD	mean	SD	ICC	95 %CI	
Centroid *x*-axis GM (%)	3.38	3.24	3.24	3.15	0.83	0.65	0.92	2.40	2.88	2.54	2.88	0.99	0.98	1.00
Centroid *x*-axis GL (%)	2.09	3.82	2.43	3.53	0.98	0.96	0.99	1.86	3.01	2.18	3.34	0.98	0.96	0.99
Centroid *y*-axis GM (%)	−3.06	3.58	−3.36	3.79	0.98	0.95	0.99	−3.76	3.36	−4.08	3.69	0.98	0.95	0.99
Centroid *y*-axis GL (%)	−1.15	3.86	−1.26	3.79	0.98	0.97	0.99	1.27	4.12	1.45	4.40	0.99	0.98	1.00

SD: mean standard deviation. ICC: intraclass correlation coefficient. 95%CI: 95% confidence interval. GM: gastrocnemius medialis muscle. GL: gastrocnemius lateralis muscle.

Table 2
Mean ± standard deviation values for the control session at each time point in both stretched and contralateral non-stretched limb.

	Stretched limb				Contralateral non-stretched limb			
	PRE	POST	POST 5	POST 10	PRE	POST	POST 5	POST 10
ROM (°)	22.60 ± 5.10	23.20 ± 6.28	23.20 ± 6.73	22.32 ± 6.13	23.69 ± 5.56	23.89 ± 5.87	23.94 ± 5.77	23.96 ± 5.70
Torque (Nm)	156.58 ± 29.12	157.13 ± 30.07	156.19 ± 29.19	157.03 ± 29.55	157.00 ± 28.57	157.30 ± 29.45	157.68 ± 29.24	158.02 ± 30.45
sEMG RMS GM (mV)	0.54 ± 0.17	0.55 ± 0.16	0.54 ± 0.17	0.52 ± 0.15	0.57 ± 0.17	0.59 ± 0.15	0.56 ± 0.16	0.58 ± 0.16
sEMG RMS GL (mV)	0.57 ± 0.17	0.58 ± 0.17	0.58 ± 0.18	0.60 ± 0.20	0.62 ± 0.20	0.62 ± 0.17	0.60 ± 0.18	0.63 ± 0.16
M−Wave GM proximal (mV)	3.86 ± 1.37	3.91 ± 1.36	3.88 ± 1.34	3.92 ± 1.32	3.86 ± 1.32	3.85 ± 1.38	3.92 ± 1.34	3.93 ± 1.33
M−Wave GM distal (mV)	3.89 ± 1.33	3.91 ± 1.35	3.90 ± 1.37	3.90 ± 1.32	3.89 ± 1.32	3.88 ± 1.35	3.85 ± 1.35	3.92 ± 1.33
M−Wave GL proximal (mV)	3.86 ± 1.37	3.91 ± 1.36	3.88 ± 1.34	3.92 ± 1.32	3.29 ± 1.15	3.23 ± 1.13	3.26 ± 1.15	3.23 ± 1.08
M−Wave GL distal (mV)	3.25 ± 1.13	3.27 ± 1.14	3.26 ± 1.14	3.26 ± 1.14	3.26 ± 1.12	3.25 ± 1.14	3.26 ± 1.14	3.24 ± 1.11
Centroid *x*-axis GM (%)	3.44 ± 3.23	3.28 ± 3.15	3.32 ± 3.17	3.20 ± 3.27	2.52 ± 3.10	2.42 ± 2.91	2.28 ± 2.76	2.67 ± 2.97
Centroid *x*-axis GL (%)	2.16 ± 3.61	2.53 ± 3.35	2.14 ± 4.21	2.32 ± 3.95	1.74 ± 3.05	1.95 ± 3.28	1.98 ± 3.12	2.41 ± 3.49
Centroid *y*-axis GM (%)	−3.02 ± 3.63	−3.20 ± 3.73	−3.10 ± 3.93	−3.52 ± 3.97	−3.83 ± 3.23	−4.19 ± 3.74	−3.66 ± 3.64	−3.97 ± 3.75
Centroid *y*-axis GL (%)	−0.94 ± 3.98	−1.16 ± 3.66	−1.37 ± 3.98	−1.39 ± 4.09	−1.25 ± 4.12	−1.41 ± 4.35	−1.30 ± 4.24	−1.49 ± 4.50

ROM: range of motion. sEMG: surface electromyography. RMS: root mean square. GM: gastrocnemius medialis muscle. GL: gastrocnemius lateralis muscle. The centroid spatial coordinates are presented as a percentage relative to the center (0) of the HD-sEMG matrix along the x (cranio-caudal) and y (medio-lateral) axis.

3.6. VAS

VAS values are shown in Fig. 8A. The Friedman's test retrieved significant differences ($P = 0.01$). However, multiple comparisons adjusted for Bonferroni's correction did not detect any significant differences (*P*-range: 0.35 – 1.00).

3.7. GM muscle architecture

Concerning fascicle length, the ANOVA-RM disclosed no *elongation* × *muscle portion* interaction ($F_{2.53} = 0.38$, $P = 0.77$, $\eta_p^2 = 0.009$, *small*). A main effect for *elongation* ($F_{2.53} = 27.25$, $P < 0.001$, $\eta_p^2 = 0.39$, *large*) was found. Irrespective of muscle portion, the fascicles were lengthened during the first elongation ($P < 0.001$ for all comparisons, $ES = 1.23$ to 2.36, *large* to *very large*), showing a similar behavior throughout the other two elongations (Fig. 8B). Concerning fascicle angle, the ANOVA-RM retrieved no *elongation* × *muscle portion* interaction ($F_3 = 0.25$, $P = 0.86$, $\eta_p^2 = 0.006$, *small*). However, a main effect for *elongation* was retrieved ($F_3 = 11.53$, $P < 0.001$, $\eta_p^2 = 0.21$, *large*). The fascicle angle decreased during the first elongation ($P < 0.001$ for all comparisons, $ES = -0.78$ to -1.51, *moderate* to *large*) independently from muscle portion, maintaining similar values until the last elongation (Fig. 8C).

4. Discussion

The study aimed to assess whether a 5-min acute PS intervention could alter the spatial distribution of muscle excitation, indicated by the centroid coordinates of the HD-sEMG matrix, in both stretched and non-stretched homologous muscle groups. It also investigated the possible neural and mechanical origins of PS-induced changes in SDME. The results showed that PS reduced MVC and HD-sEMG RMS while inducing a similar caudal shift of the centroid coordinates in both SL and CL. In the stretched leg, this shift persisted up to 5 min post-PS in GM and up to 10 min in GL. In the contralateral limb, the shift was observed immediately after PS but did not persist. No significant changes in M_{max} were found in any muscle of either limb. Furthermore, PS induced similar architectural changes between GM proximal and distal regions. Additionally, participants reported high VAS values in both muscles, indicating a high perception of stretch intensity during PS. Collectively, these findings suggest that central neural mechanisms underlie the observed SDME shift in both limbs. However, the more prolonged effects observed in the stretched limb suggest also a potential contribution of mechanical factors in SDME during MVCs.

4.1. Effects of passive stretching

Consistent with previous studies (Coratella et al., 2021, 2023), PS increased passive ankle dorsiflexion ROM and reduced torque and HD-sEMG RMS in GM and GL of both SL and CL, with more pronounced and longer-lasting effects in SL. Specifically, in SL, HD-sEMG RMS decreased in GM only at POST, whereas in GL, the reduction persisted up to $POST_{10}$. These changes likely result from both neural and mechanical factors, differently affecting SL and CL (Behm et al., 2021c; Cè et al., 2020).

From a neural perspective, mechanical stress during PS may increase discomfort perception through enhanced afferent feedback from mechanoreceptors and nociceptors (via III- and IV-group fibers) (Behm et al., 2021b; Trajano et al., 2017). Afferent signals from muscle spindles (*via* Ia- and II-group fibers) also increase during elongation but decrease as stretch tolerance improves. These mechanisms may contribute to increases in ROM (Shigetoh et al., 2022; Støve et al., 2019), while reducing neural drive to the stretched muscle, leading to decreased force and HD-sEMG RMS (Behm et al., 2021c; Trajano and Blazevich, 2021). This neural drive reduction may involve supra-spinal structures, reduced spinal excitability, and altered motor neuron facilitation (Behm et al., 2021c; Trajano et al., 2017; Trajano and Blazevich, 2021).

Although less investigated, the neural factors acting on SL seem to play a role in explaining the stretch-induced increase in ROM and the decrease in MVC and sEMG RMS in the CL, albeit with a lower magnitude and persistence than in SL (Cè et al., 2020; Coratella et al., 2021, 2023). In particular, enhanced afferent feedback from mechanoreceptors and nociceptors may exert systemic effects, increasing stretch tolerance and reducing neural drive, potentially mediated by an increase in vagal tone after PS (Trajano and Blazevich, 2021; Wong and Figueroa, 2021). Since no stretching was applied to CL, mechanical contributors can be ruled out.

Mechanically, the increased ROM and reduced MVC after PS can be primarily attributed to a decrease in whole-joint stiffness, influenced by changes in: (i) the interaction between actin and myosin filaments; (ii) non-contractile proteins within the endosarcomeric and exosarcomeric cytoskeleton; and (iii) the viscoelastic properties of connective tissue within and surrounding the muscle (Gajdosik, 2001). Additionally, modifications in titin properties may contribute to the reduction in muscle force following PS (Behm et al., 2021c).

4.2. Stretch-induced changes in spatial distribution of muscle excitation (SDME)

Together with an overall reduction in HD-sEMG RMS amplitude, we

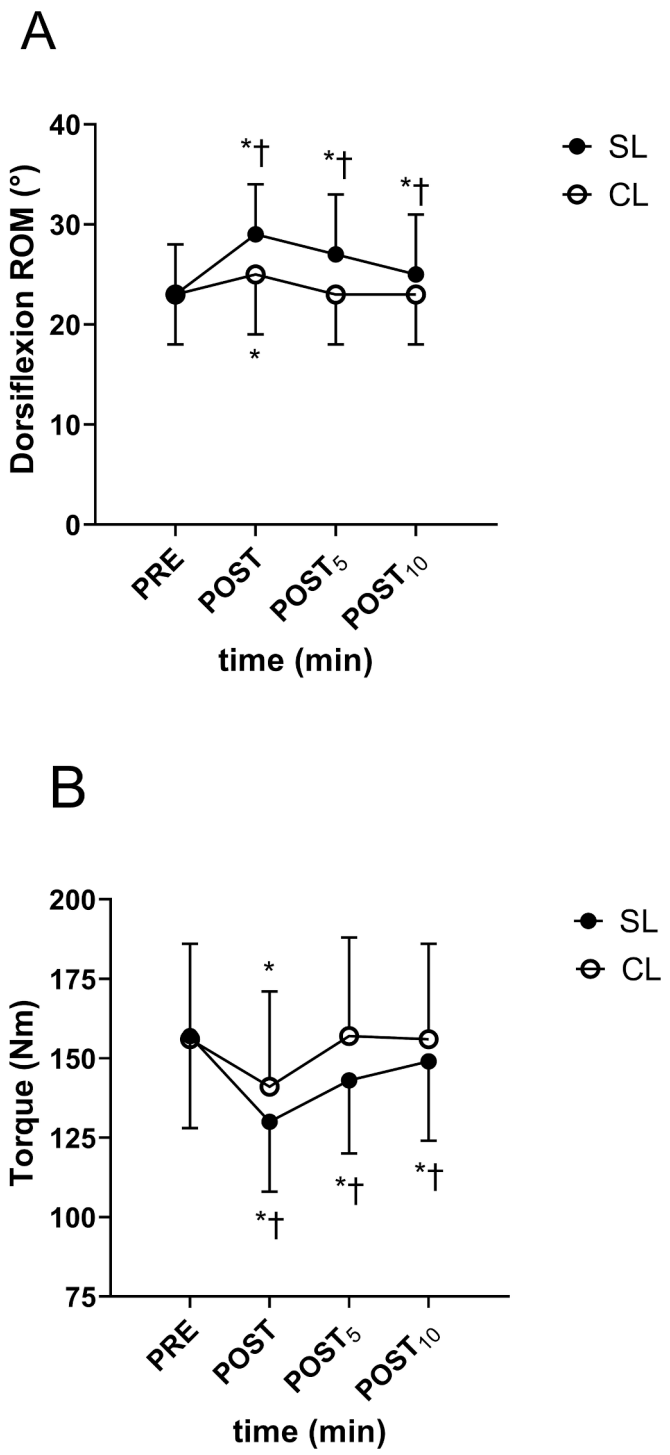

Fig. 4. Mean absolute changes in range of motion (ROM, panel A) and torque (panel B) at each time point in the stretched limb (SL) and contralateral non-stretched limb (CL) evaluations.*P < 0.05 vs. PRE. †P < 0.05 vs. CL.

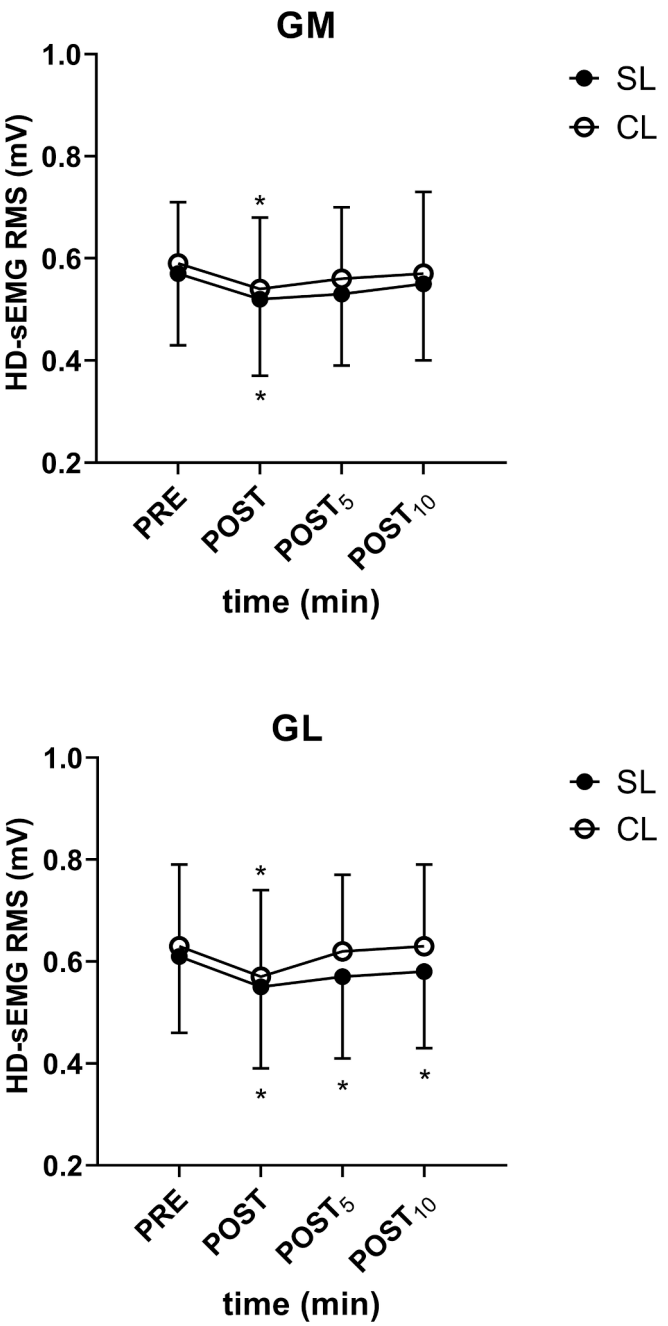

Fig. 5. Mean absolute changes in high-density surface electromyography (HD-sEMG) root-mean-square (RMS) at each time point in *gastrocnemius medialis* (GM) and *gastrocnemius lateralis* (GL) in the stretched limb (SL) and contralateral non-stretched limb (CL) evaluations.*$P < 0.05$ vs. PRE.

observed a PS-induced SDME caudal shift along the *x*-axis in both GM and GL of the stretched and contralateral non-stretched limb. In SL, this shift persisted in GM until $POST_5$, and in GL up to $POST_{10}$, while in CL it occurred until POST-only in both muscles. To our knowledge, the present study is the first to directly detect a PS-induced shift in SDME during MVCs.

Previous studies observed a muscle compartmentalization of motor units' distribution (Cohen et al., 2021; Hodson-Tole et al., 2013; Watanabe et al., 2021), although not unanimously acknowledged (Héroux et al., 2015). In the GM, motor unit recruitment exhibits task-dependent proximal–distal organization (Watanabe et al., 2021), with high-threshold units preferentially located in proximal regions compared to low-threshold units (Hodson-Tole et al., 2013). Moreover, the stretch-induced perceived discomfort during PS application could be compared to a light nociceptive stimulus (Støve et al., 2019), which, in turn, could elicit an inhibitory input by the activation of stretch-sensitive muscle-free nerve endings (Trajano and Blazevich, 2021). On these premises, SDME shift observed after PS administration could be explained by neural drive inhibition triggered by the activation of stretch-induced mechanoreceptors and nociceptors. This inhibition would primarily affect high-threshold motor units in the proximal region, reducing their firing rate and resulting in a caudal shift of the

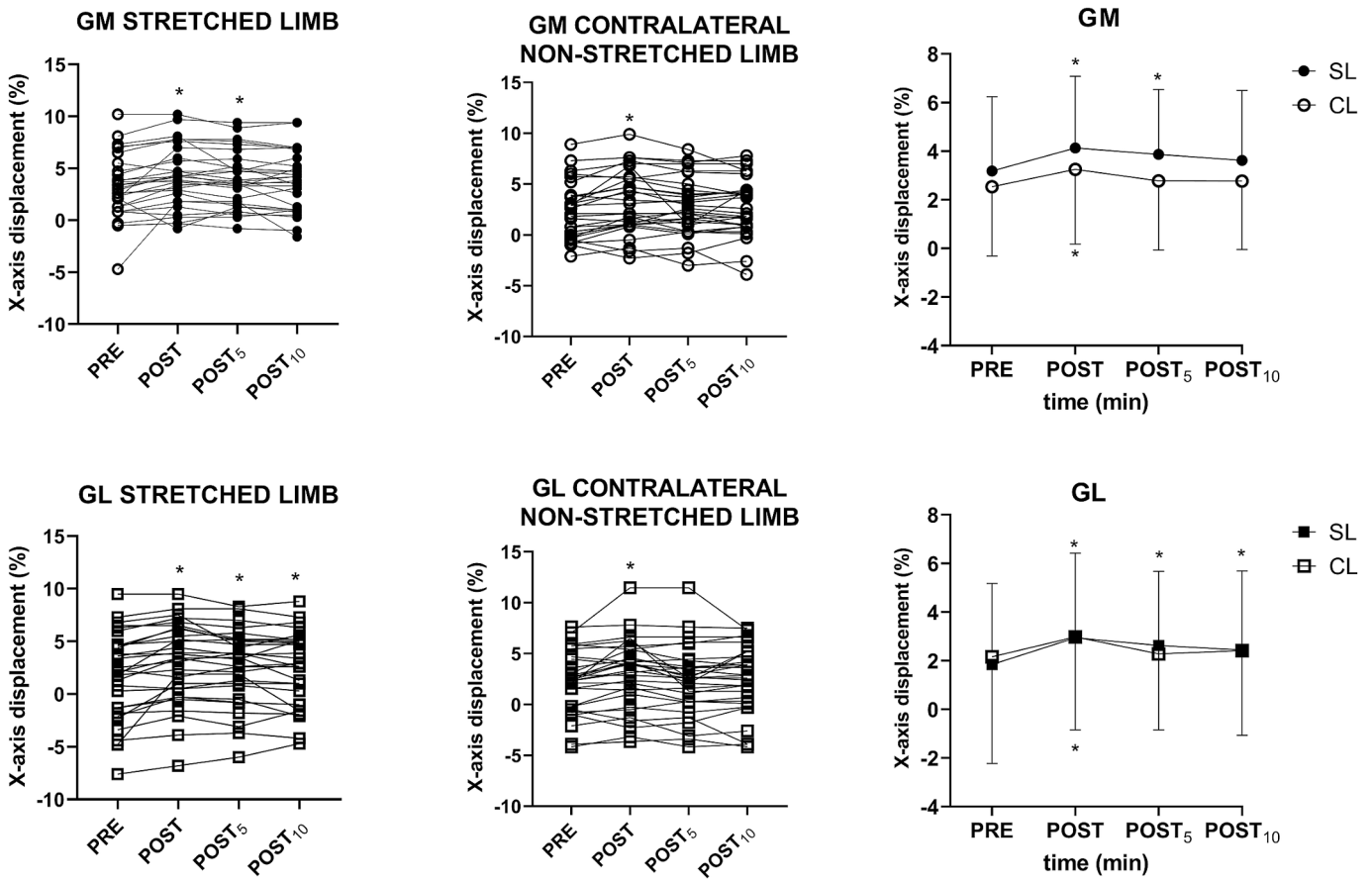

Fig. 6. Individual (panel A) and mean (panel B) spatial coordinates presented as a percentage relative to the center (0) of the high-density surface electromyography matrix along the x axis at each time point in *gastrocnemius medialis* (GM) and *gastrocnemius lateralis* (GL) in the stretched limb (SL) and contralateral non-stretched limb (CL) evaluations. *$P < 0.05$ vs. PRE.

SDME during MVCs. The inhibition caused by afferent feedback may have reduced motor drive and caused SDME caudal shift by altering the generation and transmission of motor drive across different levels: cortical, subcortical, spinal, and peripheral. Recent studies using transcranial magnetic stimulation found no changes in cortical activity after PS (Anvar et al., 2023; Pulverenti et al., 2020). Similarly, no changes at the spinal level were observed after PS (Anvar et al., 2023; Coratella et al., 2021), although this point is still under debate. Consistent with existing literature (Anvar et al., 2023; Cè et al., 2020; Coratella et al., 2021; Pulverenti et al., 2020), no M_{max} changes in all the assessed regions of both muscles and limbs were detected, suggesting that the caudal shift in SDME was not due to peripheral mechanisms such as impaired propagation of the neuromuscular action potential across the sarcolemma or issues with excitation–contraction coupling. Thus, it is likely that the stretch-induced changes in motor drive and SDME observed here would likely occur at subcortical level (e.g., basal ganglia, cerebellum, and thalamic nuclei) (Cè et al., 2020). We observed a temporal difference in the persistence of SDME alterations between GM and GL. Although data did not permit a clear explanation of this behavior, this difference might be attributed to a different management of motor drive between the two muscles (Hug et al., 2021).

Concerning CL, SDME reflected the stretch-induced inhibitory afferent feedback that may have been transferred to the contralateral hemisphere (Cè et al., 2020) through cortical and subcortical neural pathways (Carson, 2005; Wiesendanger and Wiesendanger, 1985). Furthermore, a possible predominance of the vagal tone post stretching could induce a systemic decrease in neural drive to both the stretched and non-stretched limbs through a reduction in neuromodulatory input to the motoneurons (Trajano and Blazevich, 2021).

From a mechanical perspective, heterogeneity in gastrocnemii SDME could be justified by their complex architecture, including spatial differences in fibers pennation angle and length (Aeles et al., 2022; Watanabe et al., 2021). Furthermore, it has been observed that the upper and lower portion of the *gastrocnemius* muscle exhibited different shear elastic *modulus* (an index of stiffness) during ankle dorsiflexion, measured by shear-wave elastography (Belghith et al., 2023). This behavior could implicate a different mechanical stress distribution within the same muscle, possibly resulting in an inhomogeneous lengthening of the upper and lower muscle fascicles during stretching administration. Nonetheless, all these factors could lead to a different between-region fascicle rotation during subsequent MVCs, thus resulting in redistribution of SDME (Mendez-Rebolledo et al., 2024). We did not find differences in the GM muscle fascicle elongation between the upper and lower portions during PS. However, we cannot completely rule out a potential PS-induced heterogeneous alterations in passive elastic components properties of the *gastrocnemius* muscle (Behm et al., 2021c; Morse et al., 2008), which could impact force transmission at the tendon during maximum contractions.

4.3. Study limitations

This study has several limitations. Firstly, while it is likely that central neural factors influenced the changes in SDME, the precise mechanisms responsible for the centroid shift remain unclear. The lack of direct assessment of motor unit recruitment and firing rate adaptations after stretching prevents us from distinguishing between a uniform reduction in motor drive to localized motor units and potential neuromodulation compensating for spatial differences in inhibition at the

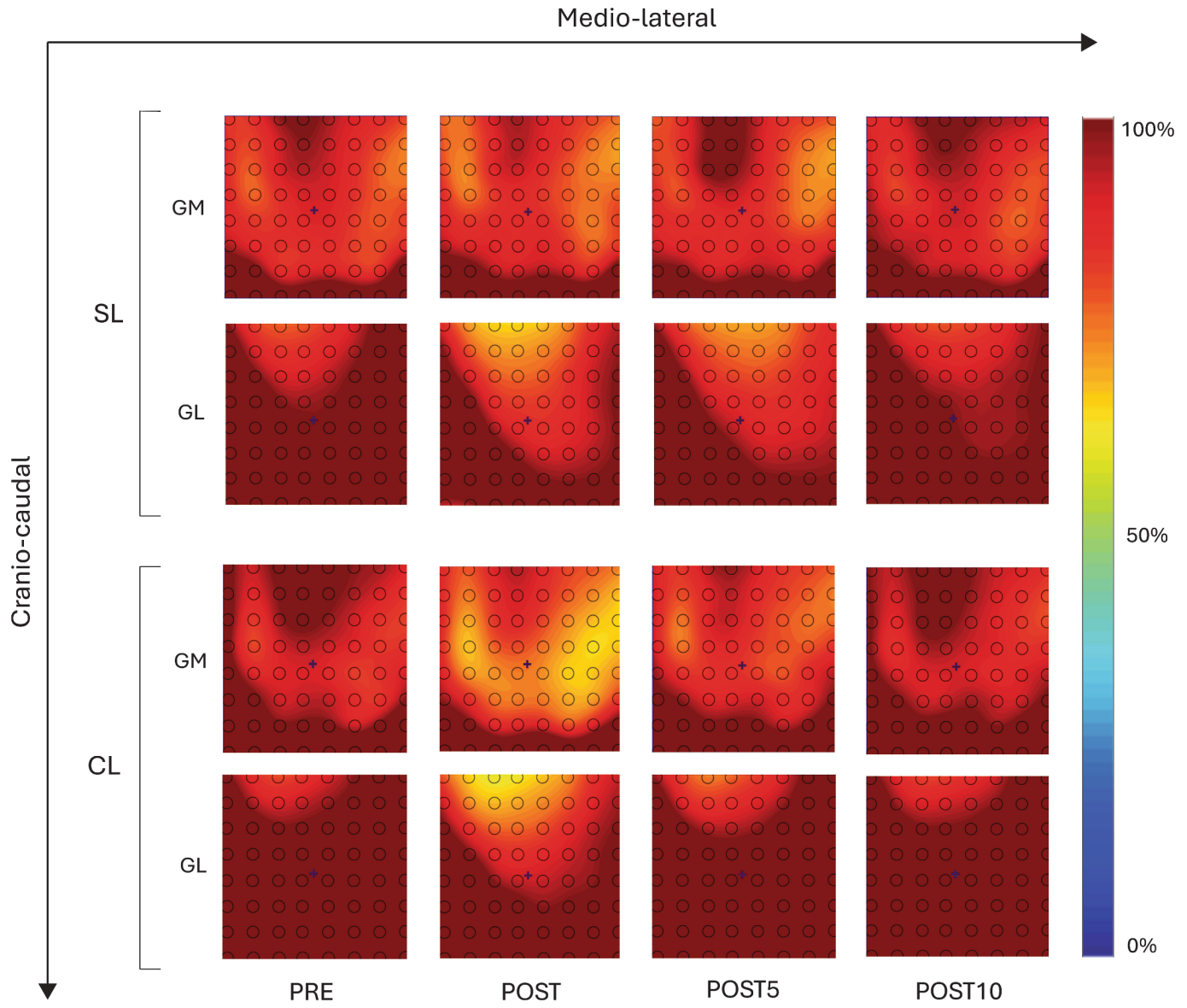

Fig. 7. G*astrocnemius medialis* (GM) and *gastrocnemius lateralis* (GL) high-density surface electromyographic activation maps of a representative participant at each time point in the stretched limb (SL) and contralateral non-stretched limb (CL) evaluations.

motor neuron pool. Furthermore, mechanically-driven changes in SDME, resulting from heterogeneous alterations in the mechanical properties of the muscle–tendon unit's parallel elastic components, cannot be entirely excluded. We also assumed similar behavior of GM and GL during the stretching protocol, although previous studies have shown comparable adaptations in fascicle length and angle between these muscles following acute (Cè et al., 2015) and chronic PS (Longo et al., 2021) using the same protocol. Nonetheless, a different acute response between these muscles cannot be excluded. Due to the placement of electrode grids over the muscle bellies, it was not feasible to assess changes in fascicle length, pennation angle, or fascicle rotation during peak MVC. Finally, different stretching modalities, durations, or intensities may yield different outcomes, warranting further research. Moreover, potential sex-related differences in the neural drive to muscle may have influenced the present results (Taylor et al., 2022). As our study included only male participants, future investigations should explore whether similar effects occur in females.

5. Conclusion

In conclusion, after PS, we observed a decrease in MVC and HD-sEMG RMS, along with a caudal shift in the centroid of SDME in both the GM and GL of the stretched limb during contraction. A similar pattern in the contralateral non-stretched limb immediately after stretching, along with the absence of differences in M_{max} between the two muscles, suggests that centrally mediated neural mechanisms primarily underlie the observed changes in spatial motor unit activity. Nonetheless, the more prolonged persistence of SDME alterations during MVCs in the stretched limb points also to the involvement of mechanical factors specific to the stretched musculature.

CRediT authorship contribution statement

Nicholas Toninelli: Writing – review & editing, Writing – original draft, Validation, Supervision, Methodology, Investigation, Formal analysis, Data curation, Conceptualization. **Giuseppe Coratella:** Writing – review & editing, Writing – original draft, Methodology, Formal analysis, Data curation. **Christian Doria:** Writing – review &

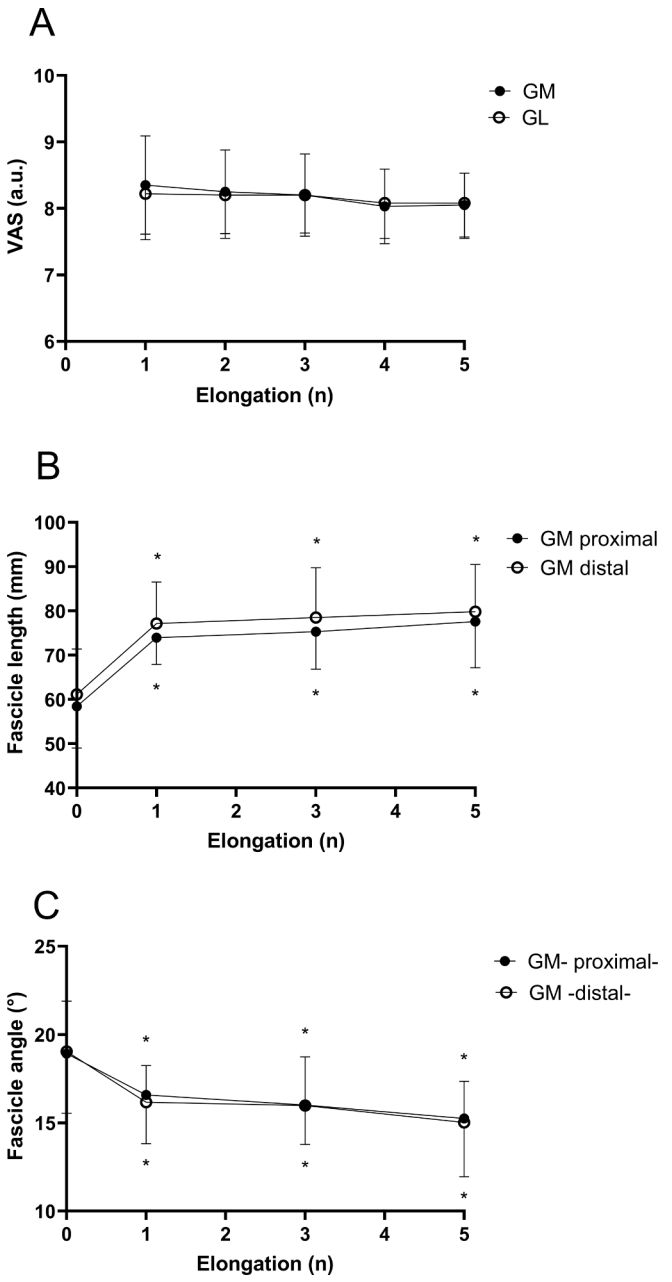

Fig. 8. Participants perception in ankle discomfort via visual analogue scale (VAS, panel A) in each passive stretching bout; proximal and distal mean absolute changes in *gastrocnemius medialis* (GM) fascicle length (panel B) and fascicle angle (panel C), measured before the maneuver and during bout #1, #3, and #5 of passive stretching. *$P < 0.05$ vs. PRE.

editing, Writing – original draft, Methodology, Formal analysis, Data curation. **Eloisa Limonta:** Writing – review & editing, Writing – original draft, Methodology, Formal analysis, Data curation. **Marta Borrelli:** Writing – review & editing, Writing – original draft, Methodology, Formal analysis, Data curation. **Susanna Rampichini:** Writing – review & editing, Writing – original draft, Methodology, Formal analysis, Data curation. **Fabio Esposito:** Writing – review & editing, Writing – original draft, Validation, Supervision, Methodology, Formal analysis, Data curation, Conceptualization. **Stefano Longo:** Writing – review & editing, Writing – original draft, Validation, Supervision, Methodology, Investigation, Funding acquisition, Formal analysis, Data curation, Conceptualization. **Emiliano Cè:** Writing – review & editing, Writing – original draft, Validation, Supervision, Methodology, Funding acquisition, Formal analysis, Data curation, Conceptualization.

Declaration of competing interest

The authors declare that they have no known competing financial interests or personal relationships that could have appeared to influence the work reported in this paper.

Acknowledgments

The authors are grateful to the participants that volunteered for the present procedures. The present study was funded by a dedicated grant (PSR Fondi Linea 2 - Tipologia A - 2020_CE) from the Department of Biomedical Sciences for Health (SCIBIS), Università degli Studi di Milano.

Appendix A. Supplementary data

Supplementary data to this article can be found online at https://doi.org/10.1016/j.jelekin.2025.103046.

Data availability

Data will be made available on request.

References

Aeles, J., Bolsterlee, B., Kelp, N.Y., Dick, T.J.M., Hug, F., 2022. Regional variation in lateral and medial gastrocnemius muscle fibre lengths obtained from diffusion tensor imaging. J. Anat. 240, 131–144. https://doi.org/10.1111/joa.13539.

Anvar, S.H., Granacher, U., Konrad, A., Alizadeh, S., Culleton, R., Edwards, C., Goudini, R., Behm, D.G., 2023. Corticospinal excitability and reflex modulation in a contralateral non-stretched muscle following unilateral stretching. Eur. J. Appl. Physiol. https://doi.org/10.1007/s00421-023-05200-9.

Barbero, M., Merletti, R., Rainoldi, A., 2012. Atlas of muscle innervation zones: Understanding surface electromyography and its applications. Springer Milan. https://doi.org/10.1007/978-88-470-2463-2.

Behm, D.G., Alizadeh, S., Drury, B., Granacher, U., Moran, J., 2021a. Non-local acute stretching effects on strength performance in healthy young adults. Eur. J. Appl. Physiol. 121, 1517–1529. https://doi.org/10.1007/s00421-021-04657-w.

Behm, D.G., Kay, A.D., Trajano, G.S., Alizadeh, S., Blazevich, A.J., 2021b. Effects of acute and chronic stretching on pain control. J. Clin. Exerc. Physiol. 10, 150–159. https://doi.org/10.31189/2165-6193-10.4.150.

Behm, D.G., Kay, A.D., Trajano, G.S., Blazevich, A.J., 2021c. Mechanisms underlying performance impairments following prolonged static stretching without a comprehensive warm-up. Eur. J. Appl. Physiol. 121, 67–94. https://doi.org/10.1007/s00421-020-04538-8.

Belghith, K., Zidi, M., Fedele, J.-M., Bou Serhal, R., Maktouf, W., 2023. Spatial distribution of stiffness between and within muscles in paretic and healthy individuals during prone and standing positions. J. Biomech. 161, 111838. https://doi.org/10.1016/j.jbiomech.2023.111838.

Bryant, J., Cooper, D.J., Peters, D.M., Cook, M.D., 2023. The effects of static stretching intensity on range of motion and strength: a systematic seview. J. Funct. Morphol. Kinesiol. 8, 37. https://doi.org/10.3390/jfmk8020037.

Campanini, I., Merlo, A., Disselhorst-Klug, C., Mesin, L., Muceli, S., Merletti, R., 2022. Fundamental concepts of bipolar and high-density surface EMG understanding and teaching for clinical, occupational, and sport applications: origin, detection, and main errors. Sensors 22, 4150. https://doi.org/10.3390/s22114150.

Carson, R.G., 2005. Neural pathways mediating bilateral interactions between the upper limbs. Brain Res. Rev. 49, 641–662. https://doi.org/10.1016/j.brainresrev.2005.03.005.

Cè, E., Coratella, G., Bisconti, A.V., Venturelli, M., Limonta, E., Doria, C., Rampichini, S., Longo, S., Esposito, F., 2020. Neuromuscular versus mechanical stretch-induced changes in contralateral versus ipsilateral muscle. Med. Sci. Sports Exerc. 52, 1294–1306. https://doi.org/10.1249/MSS.0000000000002255.

Cè, E., Longo, S., Rampichini, S., Devoto, M., Limonta, E., Venturelli, M., Esposito, F., 2015. Stretch-induced changes in tension generation process and stiffness are not accompanied by alterations in muscle architecture of the middle and distal portions of the two gastrocnemii. J. Electromyogr. Kinesiol. 25, 469–478. https://doi.org/10.1016/j.jelekin.2015.03.001.

Cohen, J.W., Vieira, T., Ivanova, T.D., Cerone, G.L., Garland, S.J., 2021. Maintenance of standing posture during multi-directional leaning demands the recruitment of task-specific motor units in the ankle plantarflexors. Exp. Brain Res. 239, 2569–2581. https://doi.org/10.1007/s00221-021-06154-0.

Coratella, G., Cè, E., Doria, C., Borrelli, M., Longo, S., Esposito, F., 2021. Neuromuscular correlates of the contralateral stretch-induced strength loss. Med. Sci. Sports Exerc. 53, 2066–2075. https://doi.org/10.1249/MSS.0000000000002677.

Coratella, G., Cè, E., Doria, C., Borrelli, M., Toninelli, N., Rampichini, S., Limonta, E., Longo, S., Esposito, F., 2023. Is the interpolated-twitch technique-derived voluntary activation just neural? novel perspectives from mechanomyographic data. Med. Sci. Sports Exerc. 55, 469–481. https://doi.org/10.1249/MSS.0000000000003076.

Dideriksen, J.L., Holobar, A., Falla, D., 2016. Preferential distribution of nociceptive input to motoneurons with muscle units in the cranial portion of the upper trapezius muscle. J. Neurophysiol. 116, 611–618. https://doi.org/10.1152/jn.01117.2015.

Falla, D., Cescon, C., Lindstroem, R., Barbero, M., 2017. Muscle pain induces a shift of the spatial distribution of upper trapezius muscle activity during a repetitive task: a mechanism for perpetuation of pain with repetitive activity? Clin. J. Pain 33, 1006–1013. https://doi.org/10.1097/AJP.0000000000000513.

Falla, D., Gallina, A., 2020. New insights into pain-related changes in muscle activation revealed by high-density surface electromyography. J. Electromyogr. Kinesiol. 52. https://doi.org/10.1016/j.jelekin.2020.102422.

Franchi, M.V., Raiteri, B.J., Longo, S., Sinha, S., Narici, M.V., Csapo, R., 2018. Muscle architecture assessment: strengths, shortcomings and new frontiers of in vivo imaging techniques. Ultrasound Med. Biol. 44, 2492–2504. https://doi.org/10.1016/j.ultrasmedbio.2018.07.010.

Gajdosik, R.L., 2001. Passive extensibility of skeletal muscle: review of the literature with clinical implications. Clin. Biomech. 16, 87–101. https://doi.org/10.1016/S0268-0033(00)00061-9.

Gifford, L.S., 1987. Circadian variation in human flexibility and grip strength. Aust. J. Physiother. 33, 3–9. https://doi.org/10.1016/S0004-9514(14)60579-1.

Héroux, M.E., Brown, H.J., Inglis, J.T., Siegmund, G.P., Blouin, J.-S., 2015. Motor units in the human medial gastrocnemius muscle are not spatially localized or functionally grouped. J. Physiol. 593, 3711–3726. https://doi.org/10.1113/JP270307.

Hirono, T., Yagi, M., Wang, Z., Sakata, H., Okada, S., Nakazato, K., Ichihashi, N., Watanabe, K., 2025. Selective static stretching of rectus femoris alters motor unit firing behaviors of knee extensors. Scand. J. Med. Sci. Sports 35, e70031. https://doi.org/10.1111/sms.70031.

Hodson-Tole, E.F., Loram, I.D., Vieira, T.M.M., 2013. Myoelectric activity along human gastrocnemius medialis: different spatial distributions of postural and electrically elicited surface potentials. J. Electromyogr. Kinesiol. 23, 43–50. https://doi.org/10.1016/j.jelekin.2012.08.003.

Hopkins, W.G., Marshall, S.W., Batterham, A.M., Hanin, J., 2009. Progressive statistics for studies in sports medicine and exercise science. Med. Sci. Sports Exerc. 41, 3–12. https://doi.org/10.1249/MSS.0b013e31818cb278.

Hug, F., Del Vecchio, A., Avrillon, S., Farina, D., Tucker, K., 2021. Muscles from the same muscle group do not necessarily share common drive: evidence from the human triceps surae. J. Appl. Physiol. 130, 342–354. https://doi.org/10.1152/JAPPLPHYSIOL.00635.2020.

Koo, T.K., Li, M.Y., 2016. A guideline of selecting and reporting intraclass correlation coefficients for reliability research. J. Chiropr. Med. 15, 155. https://doi.org/10.1016/j.jcm.2016.02.012.

Longo, S., Cè, E., Bisconti, A.V., Rampichini, S., Doria, C., Borrelli, M., Limonta, E., Coratella, G., Esposito, F., 2021. The effects of 12 weeks of static stretch training on the functional, mechanical, and architectural characteristics of the triceps surae muscle–tendon complex. Eur. J. Appl. Physiol. 121, 1743–1758. https://doi.org/10.1007/s00421-021-04654-z.

Maeda, N., Komiya, M., Nishikawa, Y., Morikawa, M., Tsutsumi, S., Tashiro, T., Fukui, K., Kimura, H., Urabe, Y., 2021. Effect of acute static stretching on the activation patterns using high-density surface electromyography of the gastrocnemius muscle during ramp-up task. Sensors 21. https://doi.org/10.3390/s21144841.

Mazzo, M.R., Weinman, L.E., Giustino, V., Mclagan, B., Maldonado, J., Enoka, R.M., 2021. Changes in neural drive to calf muscles during steady submaximal contractions after repeated static stretches. J. Physiol. 599, 4321–4336. https://doi.org/10.1113/JP281875.

Mendez-Rebolledo, G., Guzmán-Venegas, R., Cruz-Montecinos, C., Watanabe, K., Calatayud, J., Martinez-Valdes, E., 2024. Individuals with chronic ankle instability show altered regional activation of the peroneus longus muscle during ankle eversion. Scand. J. Med. Sci. Sports 34, e14535. https://doi.org/10.1111/sms.14535.

Merletti, R., Farina, D. (Eds.), 2016. Surface electromyography: physiology, engineering and applications, IEEE Press series in biomedical engineering. IEEE Press ; Wiley, Piscataway, NJ : Hoboken, New Jersey.

Morse, C.I., Degens, H., Seynnes, O.R., Maganaris, C.N., Jones, D.A., 2008. The acute effect of stretching on the passive stiffness of the human gastrocnemius muscle tendon unit. J. Physiol. 586, 97–106. https://doi.org/10.1113/jphysiol.2007.140434.

Pulverenti, T.S., Trajano, G.S., Walsh, A., Kirk, B.J.C., Blazevich, A.J., 2020. Lack of cortical or Ia-afferent spinal pathway involvement in muscle force loss after passive static stretching. J. Neurophysiol. 123, 1896–1906. https://doi.org/10.1152/jn.00578.2019.

Shigetoh, H., Nishi, Y., Osumi, M., Morioka, S., 2022. The Pain intensity/quality and pain site association with muscle activity and muscle activity distribution in patients with chronic low back pain: using a generalized linear mixed model analysis. Pain Res. Manag. 2022. https://doi.org/10.1155/2022/5751204.

Støve, M.P., Hirata, R.P., Palsson, T.S., 2019. Muscle stretching - the potential role of endogenous pain inhibitory modulation on stretch tolerance. Scand J Pain 19, 415–422. https://doi.org/10.1515/sjpain-2018-0334.

Taylor, C.A., Kopicko, B.H., Negro, F., Thompson, C.K., 2022. Sex differences in the detection of motor unit action potentials identified using high-density surface electromyography. J. Electromyogr. Kinesiol. off. J. Int. Soc. Electrophysiol. Kinesiol. 65, 102675. https://doi.org/10.1016/j.jelekin.2022.102675.

Trajano, G.S., Blazevich, A.J., 2021. Static stretching reduces motoneuron excitability: the potential role of neuromodulation. Exerc. Sport Sci. Rev. 49, 126–132. https://doi.org/10.1249/JES.0000000000000243.

Trajano, G.S., Nosaka, K., Blazevich, A.J., 2017. Neurophysiological mechanisms underpinning stretch-induced force loss. Sports Med. 47, 1531–1541. https://doi.org/10.1007/s40279-017-0682-6.

Watanabe, K., Vieira, T.M., Gallina, A., Kouzaki, M., Moritani, T., 2021. Novel insights into biarticular muscle actions gained from high-density electromyogram. Exerc. Sport Sci. Rev. 49, 179–187. https://doi.org/10.1249/JES.0000000000000254.

Wiesendanger, R., Wiesendanger, M., 1985. Cerebello-cortical linkage in the monkey as revealed by transcellular labeling with the lectin wheat germ agglutinin conjugated to the marker horseradish peroxidase. Exp. Brain Res. 59 (1), 105–117. https://doi.org/10.1007/BF00237671.

Wong, A., Figueroa, A., 2021. Effects of acute stretching exercise and training on heart rate variability: a review. J. Strength Cond. Res. 35, 1459–1466. https://doi.org/10.1519/jsc.0000000000003084.